World Journal of Engineering Research

Print ISSN: 2959-9865 Online ISSN: 2959-9873

DOI: https://doi.org/10.61784/wjer3057

DYNAMIC RESPONSE AND COUPLING MECHANISM FOR COMPOSITE FAULTS IN BEARING-BEARING SEAT SYSTEM BASED ON LS-DYNA

XingChen Wang

School of Mechanical Engineering, Xi'an Jiaotong University, Xi'an 710000, Shaanxi, China.

Corresponding Email: 2589691630@stu.xjtu.edu.cn

Abstract: This study establishes a finite element model of a 6205 rolling bearing system, incorporating the housing and central shaft, to analyze dynamic characteristics under healthy and composite fault conditions. The model's reliability is validated through close agreement between simulated and theoretical kinematic values and fault characteristic frequencies. Analysis reveals that stress concentrates at the leading edge of defects due to rolling element impact. The ball-inner ring composite fault induces the highest shear stress levels and severe fluctuations, resulting from intense interaction between moving and core load-bearing surface defects. In contrast, fixed outer ring defects cause periodic, moderate stress responses. Acceleration response analysis shows that ball-outer ring faults produce higher-amplitude, sustained vibrations due to near-rigid impacts, while ball-inner ring faults generate intermittent spikes buffered by the inner ring's inertia. These distinct signatures provide a theoretical basis for differentiating fault types in vibration signals. The findings offer accurate fault characteristics and simulation data support for vibration-based condition monitoring and early diagnosis of rolling bearings.

Keywords: Rolling bearing; Composite fault; Finite Element Analysis; Dynamic response; LS-DYNA

1 INTRODUCTION

As a core supporting component of rotating machinery, the operational status of rolling bearings directly determines the reliability and lifespan of equipment. Under complex working conditions, bearings are prone to failures such as fatigue and wear, which severely affect equipment safety [1]. Therefore, accurate modeling of their dynamic characteristics and fault analysis are of great significance.

Traditional research heavily relies on experiments and signal analysis, which are costly and struggle to capture internal contact processes. With the development of numerical simulation technology, the finite element method has become an important tool for studying bearing fault mechanisms. For instance, Zheng Tao conducted an explicit dynamic analysis of railway bearings [2]; Zhang Lele et al. revealed the influence of rolling element missing and pitting faults on stress distribution [3]; Ni Wenjun et al. identified fault characteristic frequencies through a pitting defect model [4]. Han et al. combined electromagnetic finite element analysis with measured capacitance to propose a bearing voltage prediction model [5].

However, existing studies often neglect the influence of external structures on vibration transmission. Azianou et al. pointed out that the deformation of the bearing seat alters the load distribution of deep groove ball bearings, thereby affecting fatigue life [6]. To address this, this paper establishes an integrated system model including the bearing seat and central shaft to more realistically represent actual working conditions [7]. Furthermore, research on the coupling mechanism of composite faults remains relatively scarce. Lin et al. proposed a machine tool model updating method based on dynamic evolution sequences [8], improving the accuracy of surrogate models and providing new ideas for system parameter identification. Building upon this, this paper constructs various composite fault models to systematically analyze their dynamic responses and stress characteristics. Parmar et al. employed optimized variational mode decomposition and deep learning to achieve high-precision classification of fault severity [9].

In the area of wear and life prediction, Rezaei et al. developed an adaptive finite element wear simulation method [10]; Mukras analyzed the influence of geometric parameters of journal bearings on wear [11]; Al-Tameemi et al. investigated white etching cracks induced by non-metallic inclusions [12]; Zhang et al utilized a Monte Carlo method with uniformly distributed sequences to optimize the load capacity calculation of permanent magnet bearings [13].

In summary, although current research has made significant progress in bearing fault modeling and simulation, aspects such as holistic system modeling, the coupling mechanism of composite faults, and the consideration of actual assembly and boundary conditions still require further deepening. Based on the aforementioned research findings, this paper takes the 6205 rolling bearing as the research object, establishes a system finite element model including the bearing seat, and systematically analyzes the stress distribution, vibration response, and fault characteristic frequencies under dynamic loads by configuring different types of composite faults. The aim is to provide more accurate simulation basis and methodological support for the study of bearing fault mechanisms, condition monitoring, and life prediction.

2 CONSTRUCTION OF THE FINITE ELEMENT SIMULATION MODEL FOR THE ROLLING BEARING

2.1 Geometric Parameters and Simulation Model Description

Most previous bearing simulation studies, for the sake of model simplification, have primarily modeled only the bearing itself. However, this approach inevitably fails to account for the influence of external structures surrounding the rolling bearing on vibration signal transmission. To more accurately and realistically replicate the operational conditions of the rolling bearing, this study adopts a model that incorporates a bearing seat housing the bearing and a central shaft passing through the inner ring. These three components are treated as an integrated system for finite element simulation analysis.

Considering that features such as chamfers and threaded holes on the bearing seat have a negligible impact on the simulation results while significantly increasing computational cost, this paper implements reasonable simplifications during the modeling process, as follows:

- (1) Ignore various slots, holes, and threaded holes on the bearing seat.
- (2) Omit all chamfers on the bearing seat, inner ring, and outer ring.
- (3) Set the length of the central shaft to be consistent with the width of the inner ring and treat the shaft as a rigid body.
- (4) Neglect bearing lubrication; therefore, except for the small gaps between the cage and the balls, no gaps are set between other components, and the influence of the oil film is not considered.

This study takes the 6205 bearing as the research object. The geometric parameters involved for each part in the model are shown in Table 1.

Table 1 Dimensions of 6205 Type Bearing-Bearing Seat System

Parameter	Value
Inner ring diameter D_i/mm	25
Outer ring diameter D_0/mm	52
Number of rolling elements N	9
Diameter of the ball bearing D/mm	7.94
Pitch diameter D_m/mm	38.5
Radial internal clearance $C_r/\mu m$	5
Rolling bearing width B/mm	15
Contact angle $\alpha/(^{\circ})$	0
The maximum width of the bearing housing W/mm	90
Bearing housing height H/mm	80

2.2 Mesh Generation and Defective Bearing Model Setup

Mesh generation is a critical preliminary step in finite element simulation analysis, as it directly influences the reliability of the simulation results. Generally, a smaller mesh size leads to higher model precision and more accurate simulation outcomes. However, reducing the mesh size exponentially increases computational demands. For instance, decreasing the mesh size of the inner ring in the rolling bearing model from 0.5 mm to 0.3 mm is estimated to increase the solution time by more than threefold. Therefore, selecting an appropriate mesh size that ensures model accuracy while making rational use of computational resources is particularly important.

For the moving components within the rolling bearing system, as well as components in relative motion and contact with each other—such as the inner ring, outer ring, cage, and rolling elements, which are treated as primary components—this study employs finer mesh elements. The rolling elements are the core moving parts of the rolling bearing, connecting the inner and outer rings. Consequently, the mesh element sizes for the rolling elements, inner ring, outer ring, and cage are controlled within 0.5 mm to ensure the established simulation model achieves the necessary accuracy for faithfully reflecting actual kinematic conditions. For fixed components like the bearing seat and central shaft, which have a secondary influence on the simulation results, a coarser mesh can be applied. Their element sizes are set at approximately 2 mm. In summary, the constructed bearing-bearing seat system simulation model comprises 542,665 elements and 109,561 nodes. Subsequent data verification confirms that this mesh meets the precision requirements for the simulation experiments. The meshed model is shown in Figure 1.

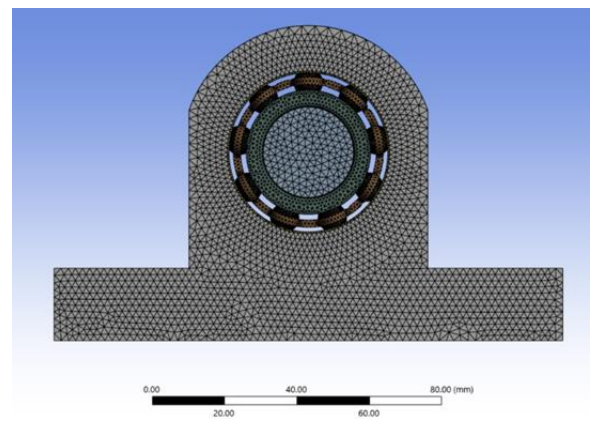
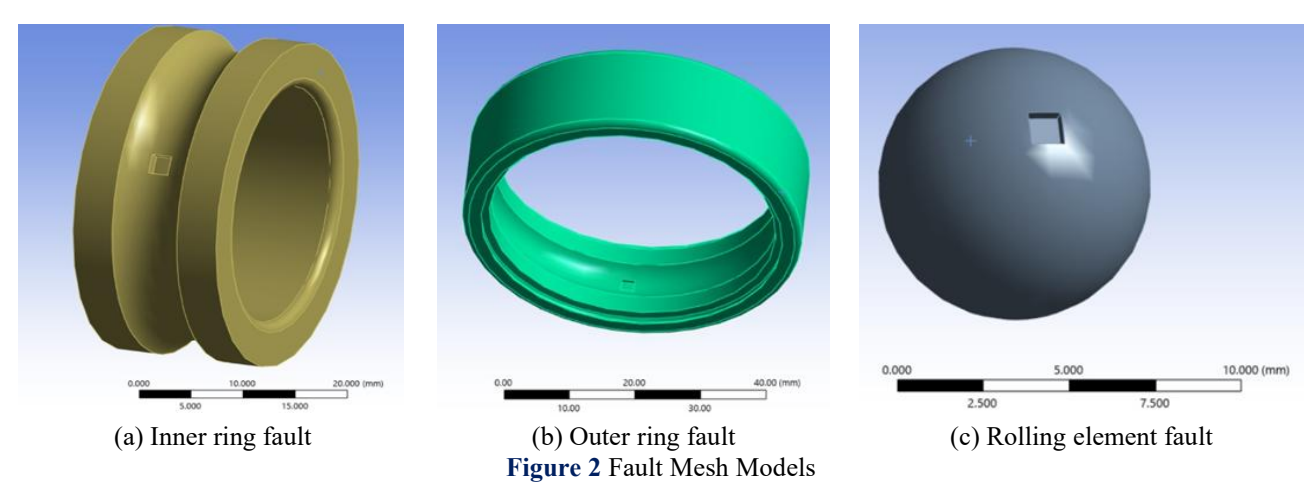


Figure 1 Meshed Model

In practical operating conditions, failures in rolling bearings can often be attributed to multiple factors such as improper installation procedures, harsh environmental conditions, and long-term overload operation. Common failure types include scratches and fatigue wear. Given the characteristics of bearings, the raceways of the inner and outer rings and the surfaces of the balls are the most prone to failure. Influenced by a combination of various factors, the specific morphology and dimensions of defect areas exhibit significant uncertainty, making it nearly impossible to precisely simulate all potential defect shapes. However, since the size of the defects is very small relative to the entire model, and the research focus of this paper is on the various manifestations of rolling bearings in the presence of defects, a representative defect model can be employed to characterize the fault features of rolling bearings. This approach is valid provided the model accurately reflects the core dynamic behaviors and typical manifestations under faulty conditions. This paper establishes finite element models for the healthy state, ball-inner ring composite fault, ball-outer ring composite fault, and inner ring-outer ring composite fault. The fault morphology is uniformly defined as a rectangular pit of 2mm × 2mm, thereby constructing bearing fault mesh models with damage to different components. The relevant fault mesh models are presented in Figure 2.



2.3 Material Parameters and Load/Boundary Condition Setting

To ensure that the established bearing-bearing seat system simulation model accurately reflects the actual operational state, it is essential to ensure that all parameters of the simulation model are fully consistent with the actual working conditions. Based on the genuine material properties of the actual 6205 bearing, this paper selects GCr15 bearing steel for the inner ring, outer ring, and rolling elements of the rolling bearing. The cage employs carbon steel, while the bearing seat is made of cast iron HT150. The corresponding materials and their parameters for each component are listed in Table 2.

Table 2 Material Parameters of Bearing-Bearing Seat System

Table 2 Waterial I arameters of Bearing Bearing Seat System				
Name of parts	Name of the material	Density $ ho(kg/mm^3)$	Elasticity modulus E/Gpa	Poisson's ratio μ
Retainer	Carbon steel	$7.83\! imes\!10^{-6}$	196	0.24
Bearing seat	Cast iron HT150	$7.15\! imes\!10^{-6}$	116	0.19
Inner ring	GCr15	$7.83\! imes\!10^{-6}$	206	0.3

Outer ring	GCr15	$7.83\! imes\!10^{-6}$	206	0.3
Rolling elements	GCr15	$7.83\! imes\!10^{-6}$	206	0.3

Due to the frictional forces acting on the rolling elements during motion, the static friction coefficient f_s and the dynamic friction coefficient f_D for the various contact interfaces are set as shown in Table 3. Furthermore, during the contact definition, a decay coefficient of 0.00001 is defined to govern the transition between the static and dynamic friction coefficients.

Table 3 Frictional Co	oefficient
------------------------------	------------

	Inner surface of outer ring	Outer surface of inner ring	Retaining cage pockets
Rolling elements	$f_{\scriptscriptstyle S}{=}0.1$	$f_{\scriptscriptstyle S}{=}0.1$	$f_{\scriptscriptstyle S} = 0.002$
Rolling elements	$f_{\scriptscriptstyle D}{=}0.1$	$f_{\scriptscriptstyle D}\!=\!0.05$	$f_{\scriptscriptstyle D}{=}0.001$

The contact between the bearing housing and the outer ring, as well as between the inner ring and the central shaft, is defined as a tied contact. The inner ring is designated as a rigid body. This configuration allows the application of rigid body forces and angular velocities directly to the inner ring, which more accurately represents actual operating conditions compared to applying forces directly to the inner ring itself. Furthermore, since LS-DYNA cannot output various data for rigid bodies, this approach offers the additional advantage of enabling the observation of data such as the deformation and acceleration of the inner ring, thereby facilitating a more comprehensive subsequent analysis of the model.

During the setup, the bottom surface of the bearing housing is fixed. The inner ring is constrained in its rotational degrees of freedom about the x and z axes, as well as its translational degree of freedom along the x-axis. Given that the forces on the cage are relatively small, it is only constrained in its rotational degrees of freedom about the x and z axes. Simultaneously, a downward radial load of 2000 N is applied to the inner ring, with a rotational speed set to 1750 r/min. The angular velocity is applied in a gradually increasing manner from 0 to 0.01 s, maintaining constant speed and load from 0.01 to 0.1 s. The total simulation duration is set to 0.1 s.

2.4 Model Reliability Verification

2.4.1 Kinematic characteristics validation

Assuming the rolling elements undergo pure rolling motion within the raceways of the inner and outer rings, the reliability of the model can be validated by analyzing the velocities of its moving components. Since the influence of defects on velocity is negligible, this section uses the healthy rolling bearing as an example to analyze the velocity of its various moving parts. Specific nodes on the inner ring and the cage of the simulation model were selected, and their velocity curves were extracted. The velocity curves of the respective components obtained from the simulation results are shown in Figure 3 and Figure 4.

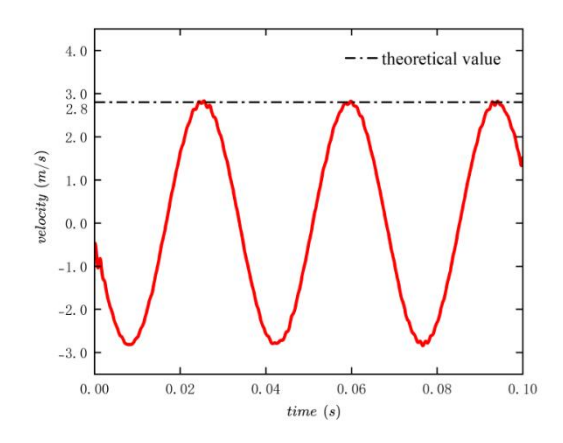


Figure 3 Inner Ring Speed Curve

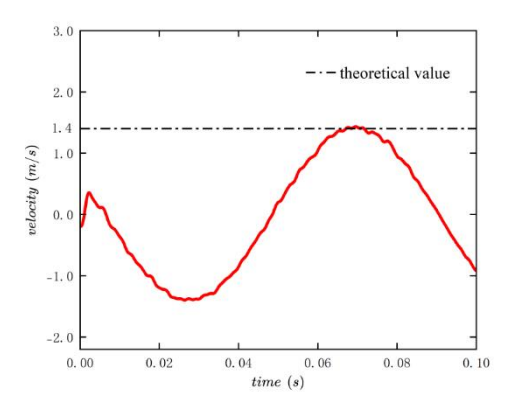


Figure 4 Retainer Speed Curve

Assuming the linear velocity at the center of the rolling element is equal to the tangential linear velocity of the cage. The theoretical calculation formulas for the tangential linear velocity of the cage v_m and the linear velocity at the inner surface of the inner ring v_i in a healthy ball bearing are given by:

$$v_m = \frac{\pi}{120} \left[n_i (D_m - D\cos\alpha) + n_0 (D_m + D\cos\alpha) \right] \tag{1}$$

$$v_i = \frac{\pi n_i}{60} (D_m - D\cos\alpha) \tag{2}$$

Since the outer ring is bonded and fixed to the bearing housing, its rotational speed $n_0=0$. The inner ring, bonded to the central shaft, has a rotational speed of 1750 r/min. According to Eq. (1), the theoretical linear velocity of the cage is calculated as $v_m=1.4m/s$. It can be observed from Figure 2-3 that this theoretical value of the cage linear velocity is very close to the peak value of the cage velocity curve obtained from the simulation. Similarly, the theoretical linear velocity at the inner surface of the inner ring, calculated using Eq. (2), is $v_i=2.8m/s$. Figure 2-4 shows that this theoretical value closely matches the peak value of the inner ring velocity curve. These results indicate that the simulated velocities of both the balls and the inner ring in the ball bearing model meet the requirements of the theoretical calculations. Therefore, the established dynamic finite element model is reliable, the simulation successfully replicates the rotational speeds, and the model can be used for analyzing the dynamic characteristics of the bearing.

2.4.2 Fault characteristic frequency validation

Validation based solely on velocity is insufficient to fully demonstrate the model's reliability. As previously established, finite element simulation models have been created for the healthy state, as well as for composite faults involving the inner-outer ring, ball-inner ring, and ball-outer ring. To simulate the process of acquiring vibration signals via sensors under practical conditions, this study extracts the vertical acceleration vibration signals from the ensemble of nine balls for all four finite element models representing different health states. Envelope analysis is performed on the vibration acceleration signals collected from the simulation to obtain the fault characteristic frequencies of the 6205 bearing. The formulas for calculating the fault characteristic frequencies of the main components of the rolling bearing are as follows:

Outer ring fault characteristic frequency:

$$f_0 = \frac{n}{2 \times 60} \left(1 - \frac{D}{D_m} \cos \alpha \right) N \tag{3}$$

Inner ring fault characteristic frequency:

$$f_i = \frac{n}{2 \times 60} \left(1 + \frac{D}{D_m} \cos \alpha \right) N \tag{4}$$

Ball fault characteristic frequency:

$$f_b = \frac{n}{2 \times 60} \frac{D_m}{D} \left(1 - \frac{D^2}{D_m^2} \cos^2 \alpha \right) N \tag{5}$$

According to Eq. (3), Eq. (4), and Eq. (5), the calculated fault characteristic frequencies are as follows: the outer ring fault characteristic frequency $f_0 = 104.2 Hz$, the inner ring fault characteristic frequency $f_i = 153.8 Hz$, and the ball fault characteristic frequency $f_b = 67.7 Hz$.

The frequency spectrum for the composite ball-inner ring fault is shown in Figure 5.

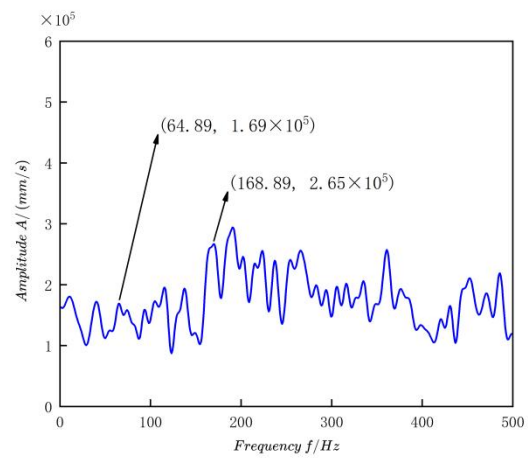


Figure 5 Frequency Spectrum for Ball-Inner Ring Fault

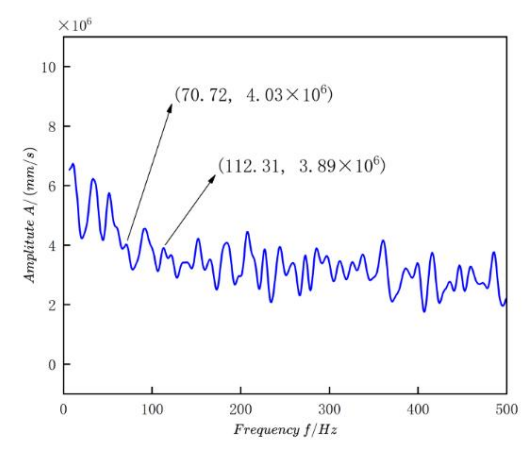


Figure 6 Frequency Spectrum for Ball-Outer Ring Fault

As shown in Figure 5, for the ball-inner ring composite fault, the simulated characteristic frequencies are 64.89 Hz and 168.89 Hz. These closely match the theoretically calculated frequencies of 67.7 Hz and 158.3 Hz, with corresponding errors of 4.15% and 6.69%, respectively.

The frequency spectrum for the composite ball-outer ring fault is shown in Figure 6.

As shown in Figure 6, for the ball-outer ring composite fault, the simulated characteristic frequencies are 70.72 Hz and 112.31 Hz. These closely match the theoretically calculated frequencies of 67.7 Hz and 104.2 Hz, with corresponding errors of 4.46% and 7.78%, respectively.

The frequency spectrum for the inner ring-outer ring composite fault is shown in Figure 7.

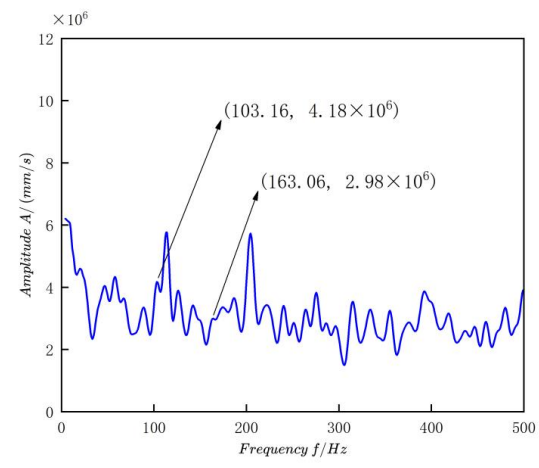


Figure 7 Frequency Spectrum for the Inner Ring-Outer Ring Composite Fault

As shown in Figure 7, for the inner ring-outer ring composite fault, the simulated characteristic frequencies are 163.06

Hz and 103.16 Hz. These closely match the theoretically calculated frequencies of 158.3 Hz and 104.2 Hz, with corresponding errors of 3.00% and 1.00%, respectively.

These results demonstrate that the simulated fault characteristic frequencies from the model constructed in this study are all close to the theoretical values under different composite fault conditions, further verifying its reliability.

3 MOTION CHARACTERISTICS FOR BEARINGS WITH DIFFERENT FAULTS

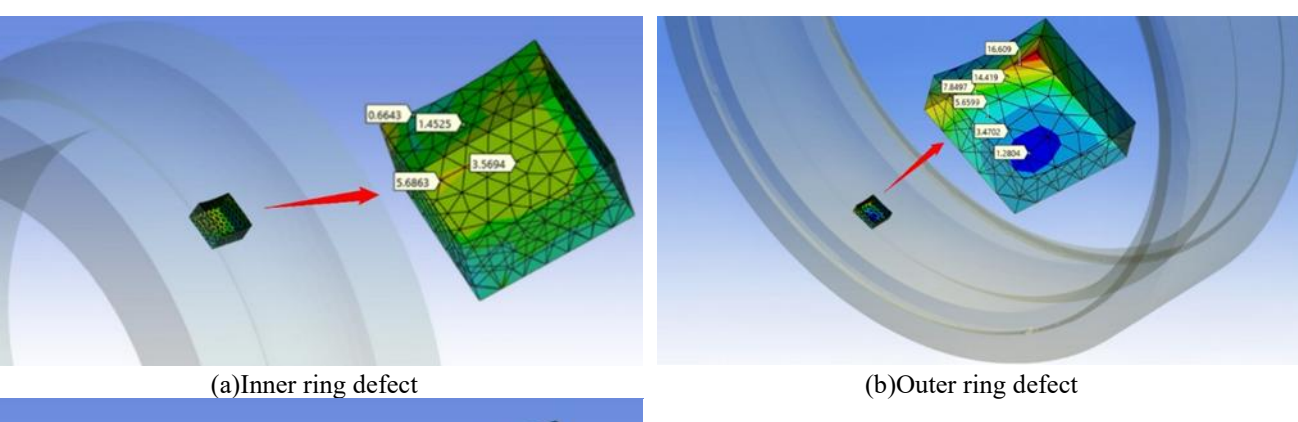
3.1 Shear Stress Variation Characteristics

3.1.1 Stress analysis at defect sites

During the operation of the bearing, the rotational motion of the inner ring and the balls generates stress on the contact surfaces between the balls and the bearing raceways [14]. Therefore, analyzing the shear stress in the contact area provides insight into the mechanical state within the bearing during operation.

The shear stress contour plots at the three different defect locations are shown in Figure 8.

From the stress contour plots in Figure 8, it can be observed that the shear stress across the entire defect surface is not uniformly distributed along the five inner surfaces of the rectangular pit. Instead, a distinct stress concentration zone is evident on the bottom surface, biased towards one direction. This occurs because, during the motion of the balls, the leading edge of the defect consistently bears the load first. Consequently, the maximum shear stress at the leading edge of the pit defect is greater than that at the trailing edge. Regarding the overall stress distribution within the defect, the stressed area exhibits a gradual decreasing trend radiating outward from the edges of the defect. Furthermore, the absolute maximum stress for the entire defect is consistently located at the intersection line between the wall and the bottom surface at the defect's leading edge. This phenomenon arises because when a ball passes the leading edge of the defect at a relatively high velocity, it compresses the wall at the leading edge downwards, thereby inducing significant stress concentration at the base of the wall.



11.402 0.485

(c)Ball defect

Figure 8 Shear Stress Contour Plots at the Three Different Defect Locations

3.1.2 Impact of composite defects on the overall shear stress of the bearing

The preceding analysis has clearly revealed the characteristics and formation mechanisms of stress concentration at individual local defect sites. To investigate the more complex mechanical behaviors under the coupled effects of multiple faults, this study expands the analytical perspective from the local defect to the entire bearing system. The following section will systematically compare the distribution and dynamic fluctuation characteristics of shear stress across the entire bearing under three different composite defect models. The focus is on elucidating the differences in the interaction and superposition of stress fields induced by different types of composite defects, which consequently produce more significant global impacts compared to single defects. It also aims to deeply reveal the synergistic

mechanism of this multi-fault coupling on the overall mechanical performance and dynamic response patterns of the bearing, thereby providing a theoretical basis for accurately assessing the hazards of composite faults in practical operating conditions.

The shear stress curves on the bearing surface for different composite defects are shown in Figure 9.

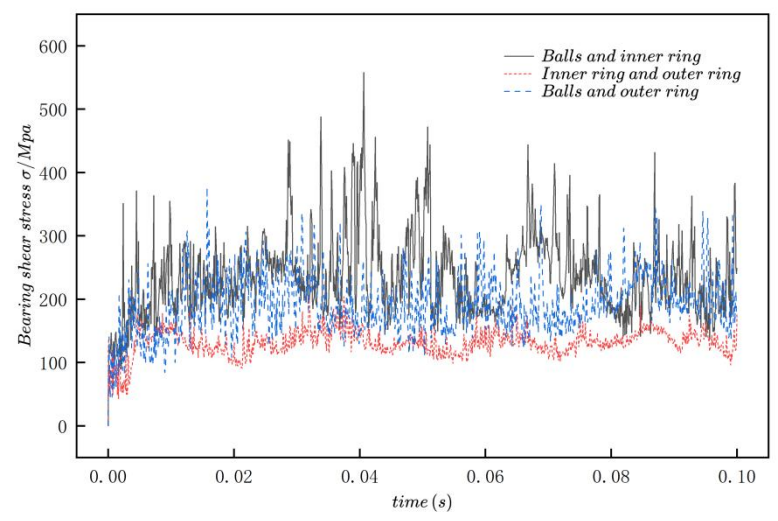


Figure 9 Shear Stress Curves on the Bearing Surface for Different Composite Defects

Regarding the overall distribution level of shear stress, the stress curve for the ball-inner ring composite defect is the highest overall, followed by the ball-outer ring defect, with the inner ring-outer ring composite defect being the lowest. This phenomenon is closely related to the load transmission path and the relative motion velocity. In the model presented in this paper, the rotating inner ring is the active driving component and the primary channel for load input. Consequently, the contact stress between the balls and the inner ring raceway is inherently the most severe. When defects are present simultaneously on both the balls and the high-speed rotating inner ring, a continuous and intense interaction is formed between the "kinematic defect" and the "core load-bearing surface" at high speed. Each contact is accompanied by significant impact, thereby substantially elevating the baseline stress level across the entire contact area. For the ball-outer ring defect, since the outer ring is fixed, its defect location is static relative to the load zone. Although it is periodically impacted by the moving ball defect, its dynamic effect is weaker than in the inner ring case. In contrast, the inner ring-outer ring composite defect, as it does not involve the ball as a source of impact, exhibits a stress response primarily stemming from the static influence of the two fixed raceway defects on the variation of the contact line, resulting in the lowest overall stress level.

In terms of stress fluctuation characteristics, defects involving balls exhibit significantly larger fluctuation amplitudes than the inner ring-outer ring defect, with the ball-inner ring condition showing the most pronounced fluctuations. This accurately reflects that kinematic defects are the primary source of dynamic excitation in the system. The revolution and rotation of the balls cause their defects to periodically impact the inner and outer ring raceways. In the ball-inner ring combination, the ball defect impacts the high-speed moving inner ring, and the extremely high relative velocity between them amplifies the severity of the impact. In the ball-outer ring combination, the ball impacts the stationary outer ring, where the relative velocity is lower; thus, the impact force and fluctuation amplitude are correspondingly reduced. The inner ring-outer ring defect, lacking such periodic sharp impact excitation, naturally exhibits the gentlest curve fluctuations.

From the perspective of curve phase, the phases of the ball-outer ring and ball-inner ring curves are similar, but both exhibit an almost anti-phase relationship with the curve of the inner ring-outer ring defect. This profoundly reveals the origin of the system's excitation mechanism. The excitation sources for the former two are essentially the "kinematic ball defect," and the impact force pulses they generate share a common phase origin. However, for the inner ring-outer ring defect, the system's vibration excitation mainly arises from the "meshing-unmeshing" effect generated when the defect on the rotating inner ring periodically passes through the load zone and interacts with the fixed outer ring defect. This excitation mode, dominated by the change in the relative position of the two fixed raceway defects, is fundamentally different in phase from the impact mode of the moving balls. Consequently, it excites different vibration patterns in the system, manifesting as a significant anti-phase characteristic.

3.1.3 Influence of different defects on stress in specific component

To thoroughly investigate the local mechanical effects of different composite fault modes on specific components, this section will conduct a comparative analysis focusing on three core load-bearing parts: the outer surface of the inner ring, the inner surface of the outer ring, and the balls. Specifically, two composite defect scenarios will be analyzed for each part. By extracting and comparing the stress data of these specific components from the three models (namely, the ball-inner ring, ball-outer ring, and inner ring-outer ring composite fault models), the aim is to identify which defect combination induces the most significant stress concentration and dynamic load on a particular component. This analysis seeks to reveal the key modes governing component damage in composite faults and their underlying

interaction mechanisms.

The shear stress curves of the balls in the ball-outer ring and ball-inner ring defect models are shown in Figure 10.

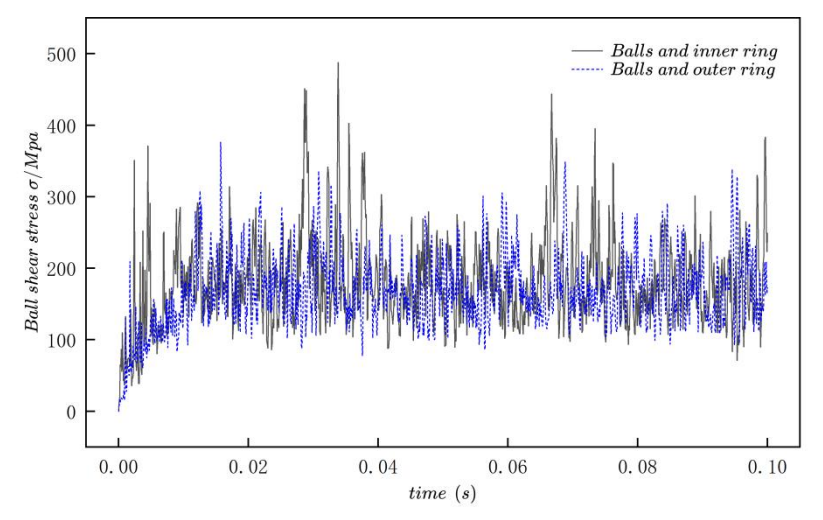


Figure 10 Shear Stress Curves of the Balls in the Ball-Outer Ring and Ball-Inner Ring Defect Models

As shown in Figure 10, during specific time intervals such as 0–0.01 s, 0.03–0.04 s, and 0.065–0.075 s, the fluctuation amplitude of the shear stress under the ball-inner ring defect condition is significantly greater than that under the ball-outer ring defect. This is primarily attributed to the higher relative velocity between the balls and the inner ring raceway under the constraint condition of "rotating inner ring and fixed outer ring." When the ball defect collides with the high-speed rotating inner ring defect, a more intense transient impact is generated. In other time intervals, the fluctuation amplitudes of the two curves are similar, indicating that when the balls are not in the main load-bearing zone or a specific contact phase, the influence of the defect type on the ball stress fluctuation is relatively diminished. During these periods, the stress response of the balls is governed more by the overall dynamic behavior of the system, causing the fluctuation levels under different defect models to converge.

Regarding the characteristics of the fluctuation distribution, the curve for the ball-inner ring condition exhibits distinct alternating features of "stress fluctuation concentration zones" and "relatively stable zones." In contrast, the fluctuations in the ball-outer ring curve lack such pronounced characteristics. This suggests that the influence of the inner ring defect on the balls possesses a stronger periodic impact nature, whereas the effect of the outer ring defect is relatively more continuous and uniform. These differences fully demonstrate that in composite fault bearings, the inner ring defect has a more significant dynamic impact on the balls and is the primary factor causing severe stress fluctuations in the balls.

The shear stress curves on the outer surface of the inner ring for the inner ring-outer ring and ball-inner ring defect models are shown in Figure 11.

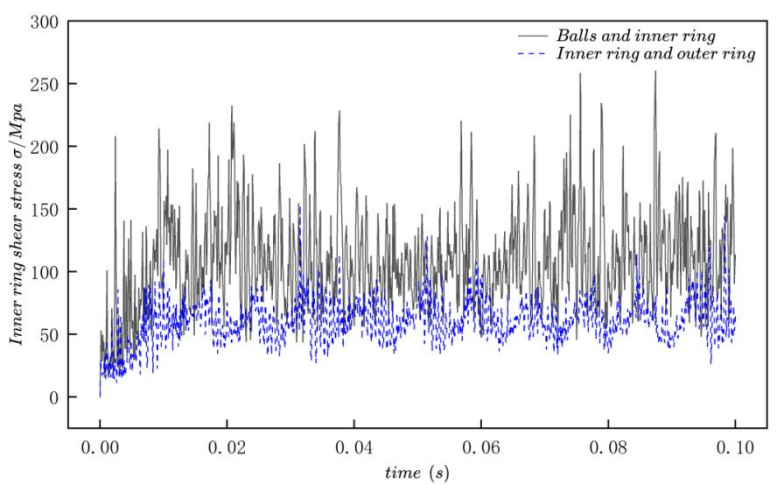


Figure 11 Shear Stress Curves on the Outer Surface of the Inner Ring

Through a comparative analysis of the shear stress on the outer surface of the inner ring in the two composite fault models (ball-inner ring and ball-outer ring), systematic differences in their stress responses due to different defect types can be clearly observed.

In terms of stress level, the shear stress curve under the ball-inner ring composite fault condition is significantly higher overall, with a maximum value reaching approximately 250 MPa, whereas the maximum value under the ball-outer ring condition is only 150 MPa. This phenomenon reveals the fundamental difference in the relative motion state between

the defect and the inner ring: the ball defect, acting as a high-speed moving impact source, generates direct and intense transient impacts on the rotating inner ring raceway, thereby substantially elevating the baseline stress level of the inner ring. In contrast, the fixed outer ring defect exerts a static and indirect influence on the system; the impact force it generates must be transmitted through the balls to act on the inner ring, resulting in some energy dissipation. Consequently, its overall effect on the stress level of the inner ring is relatively weaker.

The differences in fluctuation characteristics are also significant. Under the ball-inner ring fault condition, the fluctuation amplitude of the inner ring shear stress is markedly larger and appears random within the initial 0–0.1 s, without showing a distinct pattern. This reflects the complexity of the excitation source from the ball defect. Its impact is modulated by multiple factors including the revolution and rotation of the balls and the randomness of the defect position, leading to a non-periodic and severe fluctuating stress response in the inner ring. In stark contrast, the stress curve under the ball-outer ring fault condition exhibits stable periodic fluctuations, with clear peaks and troughs, and the interval between adjacent peaks is approximately 0.01 s. This is primarily because the fixed outer ring defect provides a periodic excitation source at a constant location, with its excitation frequency fixed at the ball pass frequency, thereby exciting a more regular and relatively gentler periodic stress response in the inner ring. In summary, the moving ball defect is the dominant factor causing severe and random stress concentration in the inner ring, whereas the static outer ring defect primarily induces a regular but moderate periodic stress fluctuation.

The shear stress curves on the inner surface of the outer ring for the inner ring-outer ring and ball-outer ring defect models are shown in Figure 12.

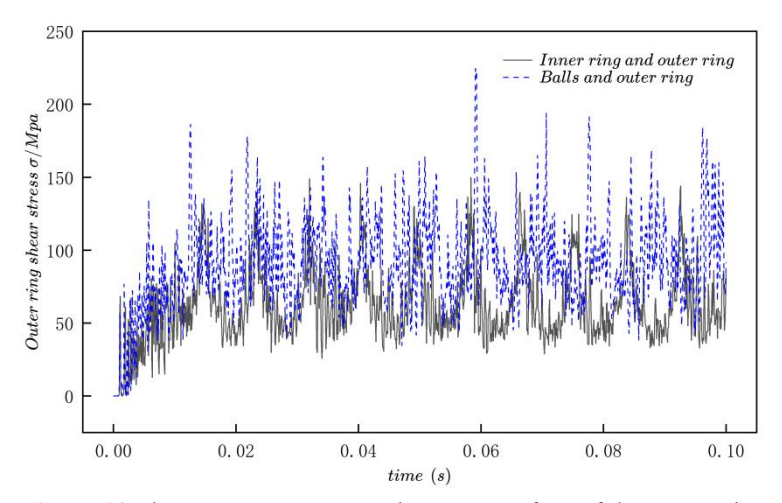


Figure 12 Shear Stress Curves on the Inner Surface of the Outer Ring

From the perspective of the overall stress distribution, the shear stress curve under the ball-outer ring composite fault condition is significantly higher than that under the inner ring-outer ring composite fault, with its maximum value reaching 200 MPa compared to only 150 MPa for the latter. The core reason for this phenomenon lies in the difference in the relative position of the defect to the fixed outer ring and the directness of the impact. The ball defect, acting as a moving impact source, directly and frontally strikes the fixed outer ring raceway during its revolution, generating extremely high transient stress at the moment of contact. In contrast, the influence of the inner ring defect on the fixed outer ring is indirect; its periodic excitation must alter the force state of the balls before being transmitted to the outer ring. This indirect transmission path dissipates part of the energy, resulting in a relatively lower perceived stress level on the outer ring.

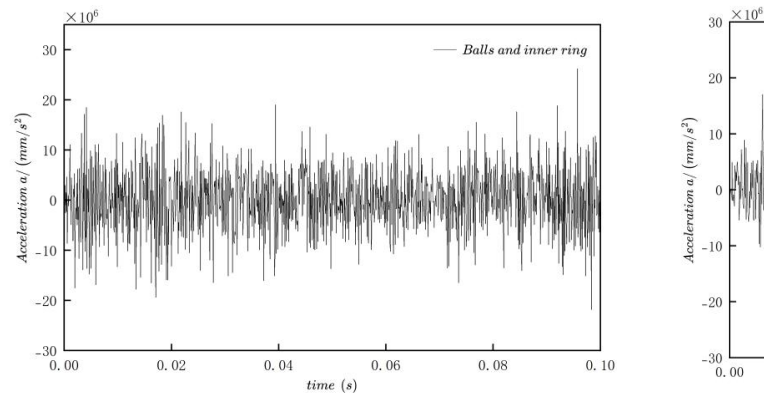
In terms of fluctuation characteristics, both defect models induce noticeable periodic fluctuations. The curves exhibit stable peaks and troughs, with adjacent intervals of approximately 0.01 s, corresponding to the characteristic frequency of the balls passing the fixed point on the outer ring. This indicates that the overall system dynamics are dominated by periodic events. A key common feature is that the stress curves of both models display a "sharp peak and convex trough" shape, meaning the duration of the troughs is significantly longer than that of the sharp peaks. This vividly reflects the force-bearing process of the bearing: the peaks represent the instantaneous impact generated when a ball, particularly one with a defect, passes by, which is short in duration but high in intensity; whereas the troughs correspond to the decay and relatively stable distribution of stress over a longer period after the impact.

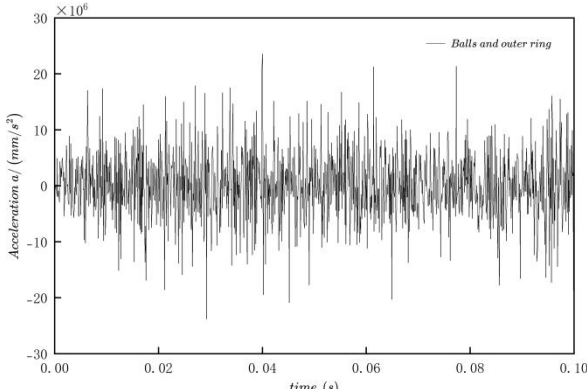
However, there are important differences in the details of their dynamic responses. Although the overall fluctuation amplitudes are not significantly different, the ball-outer ring defect curve exhibits suddenly increased peak values at specific times, such as 0.01 s, 0.06 s, and 0.1 s, compared to other moments. This accurately captures the randomness and high-intensity nature of the ball defect impacts. These anomalous peaks likely correspond to instances where a defective ball, at a specific phase (such as exactly at the center of the load zone), collides violently with the edge of the outer ring defect, generating an impact force far exceeding that of regular periodic excitations. In contrast, the curve for the inner ring-outer ring defect is relatively smoother. Its fluctuations primarily stem from changes in the relative position between the periodically passing inner ring defect through the load zone and the fixed outer ring defect, making it less prone to such abnormal stress spikes.

3.2 The Influence of Different Defects on Ball Acceleration Response

The preceding analysis of shear stress in the bearing rings and balls clearly revealed the static characteristics and stress distribution patterns under different composite fault modes. However, changes in the stress field represent only one aspect of fault manifestation. The dynamic response of the bearing during operation, particularly the acceleration signal of the balls—the core moving components—holds more sensitive features for revealing the transient characteristics of impact events and identifying fault types. To delve deeper into the differential effects of inner ring, outer ring, and ball defects on the dynamic behavior of the bearing system, this section shifts the analytical perspective from static stress to dynamic acceleration. It focuses on a comparative study of the amplitude characteristics and fluctuation patterns of the ball acceleration response in the inner ring-outer ring composite fault model and the ball-outer ring composite fault model. The aim is to further elucidate the excitation mechanisms and evolution laws of different defects from a dynamic perspective.

The acceleration curves of the balls under the ball-outer ring defect and the ball-inner ring defect conditions are shown in Figure 13.





(a) Ball-inner ring composite fault

(b)Ball-outer ring composite fault

Figure 13 Acceleration Curves of the Balls

In terms of the overall fluctuation amplitude of acceleration, the magnitude under the ball-outer ring composite fault condition is significantly greater than that under the ball-inner ring composite fault. The core reason for this phenomenon lies in the differing kinematic states of the defective components and their boundary constraints. When a ball passes a fixed outer ring defect, it is equivalent to a moving mass impacting a rigidly fixed point. The impact force generated by such a collision cannot be buffered by displacement or deformation of the defect body; the impact energy is almost entirely and instantaneously counteracted onto the ball itself, thereby exciting an acceleration response with a very high amplitude. In contrast, under the ball-inner ring fault condition, the inner ring itself is a massive, high-speed rotating inertial body. When a ball collides with an inner ring defect, part of the impact force is converted into a change in the rotational momentum of the inner ring. This inertial system absorbs and dissipates a portion of the impact energy. Consequently, the peak impact force transmitted back to the ball is attenuated, resulting in a relatively lower overall fluctuation amplitude in its acceleration response.

The temporal characteristics of the fluctuations and the distribution of peaks also exhibit distinct patterns between the two conditions:

The acceleration curve for the ball-inner ring fault shows increased amplitudes at specific instances, such as 0.002 s, 0.018 s, and 0.04 s, while remaining relatively stable during other periods. This reflects the intermittent nature of its excitation. These peaks correspond to transient impacts that occur when the phases of the ball defect and the inner ring defect coincide at specific locations within the load zone during their motion. Because both defects are moving, this intense interaction occurs only at specific relative positions, thus manifesting as intermittent high peaks superimposed on a stable background vibration.

In contrast, the acceleration curve for the ball-outer ring fault maintains large-magnitude fluctuations throughout the entire time period, with extreme amplitude values occurring at times such as 0.028 s and 0.04 s. This reveals the continuous and periodic nature of its excitation. The fixed outer ring defect acts as a periodic forced excitation source for the revolving balls. Each ball collides with it once per revolution, leading to a sustained high-amplitude response. The exceptionally high peaks observed within this response correspond to instances where the geometric phase of the ball's own defect couples with its orbital phase, causing the deepest engagement or most severe collision with the outer ring defect. This generates impact pulses that exceed those of regular periodic interactions.

This analysis demonstrates that the outer ring defect, as a fixed geometric excitation source, imposes a continuous and very high-amplitude acceleration excitation on the balls. Its dynamic response exhibits characteristics of a broad frequency band and high energy. Conversely, the inner ring defect, acting as a moving inertial excitation source, imposes intermittent and buffered impacts on the balls. Its acceleration response is characterized by periodic spikes superimposed on a stable baseline. This distinction provides a theoretical basis for fault diagnosis: in vibration signals, a

sustained, high-amplitude, broad-frequency-band acceleration response is more likely to indicate an outer ring fault, whereas periodic impact spikes are more characteristic of an inner ring fault.

4 CONCLUSION

Taking the 6205 rolling bearing as the research object, this study addressed the shortcomings of existing research in holistic system modeling and the analysis of composite fault coupling mechanisms. It successfully established a finite element model of the bearing system incorporating the bearing housing and central shaft, and systematically and thoroughly investigated the dynamic characteristics of the bearing under healthy conditions and various composite fault modes. Through simulation analysis and theoretical verification, the main conclusions drawn are as follows:

- 1. The established finite element model of the bearing-bearing seat system demonstrates high consistency between simulated values and theoretical calculations for the linear velocities of both the cage and the inner ring in terms of kinematic characteristics. In terms of fault diagnosis, the errors between simulated and theoretical characteristic frequencies under multiple composite faults are all minimal. This indicates that the model accurately replicates the actual dynamic behavior of the bearing, providing a reliable simulation platform for subsequent fault characteristic analysis.
- 2. At local defect sites, shear stress is not uniformly distributed; instead, significant stress concentration occurs at the junction of the bottom surface and the wall at the leading edge of the pit. This is caused by the squeezing effect when the rolling element passes over the defect at high speed. Regarding the overall system stress level, the ball-inner ring composite fault induces the highest shear stress and the most severe fluctuations. This is because it involves the intense interaction at high speed between both the moving impact source (ball defect) and the core load-bearing surface (inner ring defect). In contrast, the inner ring-outer ring composite fault, which does not involve a ball defect, exhibits the lowest overall stress level and fluctuation amplitude. Stress analysis on different components reveals that moving defects are the dominant factor causing severe and random stress concentration. The direct impact of a ball defect on the inner ring significantly elevates the inner ring's stress baseline and induces random fluctuations. Conversely, a fixed outer ring defect primarily leads to regular and moderate periodic stress responses.
- 3. By analyzing the acceleration response of the balls, it was found that the ball-outer ring composite fault excites acceleration fluctuations with higher amplitude and better persistence. This is because the impact from the fixed outer ring defect on the moving ball more closely resembles a rigid collision, resulting in less energy dissipation. In contrast, the acceleration response of the ball-inner ring composite fault manifests as intermittent spikes superimposed on a stable baseline. This is due to the inertial mass effect of the rotating inner ring buffers and dissipates a portion of the impact energy. This difference provides a clear theoretical basis and characteristic indicators for distinguishing between inner ring and outer ring faults in vibration signals.

In summary, through systematic simulation analysis, this paper has clarified the evolution patterns of mechanical behavior and vibration characteristics of rolling bearings under the coupled action of composite faults, deepening the understanding of bearing failure mechanisms. The research results can provide more accurate fault characteristic references and simulation data support for vibration-based bearing condition monitoring and early fault diagnosis, holding significant theoretical importance and engineering application value for improving the reliability maintenance level of rotating machinery.

Future research work could further consider lubricating conditions, thermal effects, and more complex time-varying load conditions to make the model more closely aligned with engineering reality. Simultaneously, exploring intelligent diagnosis methods based on algorithms like deep learning that integrate simulation and experimental data is recommended.

COMPETING INTERESTS

The authors have no relevant financial or non-financial interests to disclose.

REFERENCES

- [1] Junbao Yang. Research on Finite Element Modeling and Dynamic Response Characteristics of Composite Faults of Rolling Elements and Outer Raceways in Ball Bearings. Gansu: Lanzhou University of Technology, 2022.
- [2] Tao Zheng. Explicit Dynamic Simulation and Fault Feature Analysis of Railway Vehicle Bearings. Master's Thesis. Shijiazhuang: Shijiazhuang Railway University, 2014.
- [3] Lele Zhang, Nanlin Tan, Li Fan. Explicit Dynamic Simulation and Analysis of Rolling Bearing Faults. Journal of Shanghai Jiao Tong University, 2007, 41(9): 1506-1509. DOI: 10.3321/j.issn:1006-2467.2007.09.025.
- [4] Wenjun Ni, Chang Zhang, Ziyang Jiang, et al. Dynamic Characteristics Analysis of Ball Defect Bearings Based on LS-DYNA and Refinement Spectrum Bearing. 2024.
- [5] Han P, Heins G, Patterson D, et al. Modeling of bearing voltage in electric machines based on electromagnetic FEA and measured bearing capacitance. IEEE Transactions on Industry Applications, 2021, 57(5): 4765-4775.
- [6] Ayao E Azianou, Karl Debray, Fabrice Bolaers, et al. Modeling of the Behavior of a Deep Groove Ball Bearing in Its Housing. Journal of Applied Mathematics and Physics, 2013, 1: 45-50. DOI: 10.4236/jamp.2013.14009.
- [7] Dong Lian. Research on Dual-domain Adaptive Fault Diagnosis of Rolling Bearings Based on Dynamic Simulation Data. Beijing: Beijing University of Chemical Technology, 2024.

- [8] Lin W, Zhong P, Wei X, et al. Machine tool FEM model correction assisted by dynamic evolution sequence. Scientific Reports, 2025, 15: 18789. DOI: 10.1038/s41598-025-03058-9.
- [9] Vivek Parmar, Shirshendu Layek, Megha Bhushan, et al. Advanced deep learning approach for the fault severity classification of rolling-element bearings. Scientific Reports, 2025, 15: 34353. DOI: 10.1038/s41598-025-16895-5
- [10] Rezaei A, Van Paepegem W, De Baets P, et al. Adaptive finite element simulation of wear evolution in radial sliding bearings. Wear, 2012, 296(1-2): 660-671.
- [11] Mukras S M S. Influence of Geometric Parameters on Journal Bearing Wear: A Finite Element Analysis and Elastic Foundation Approach. Applied Sciences, 2025, 15(5): 2368.
- [12] Al-Tameemi H A, Long H. Finite element simulation of subsurface initiated damage from non-metallic inclusions in wind turbine gearbox bearings. International Journal of Fatigue, 2020, 131: 105347.
- [13] Zhang L, Wu H, Li P, et al. Design, analysis, and experiment of multiring permanent magnet bearings by means of equally distributed sequences based Monte Carlo method. Mathematical Problems in Engineering, 2019, 2019(1): 4265698.
- [14] Wenjun Ni, Chang Zhang. Dynamic Characteristics Analysis of Defective Bearings Based on Simulation Dynamics Model. Journal of Mechanical & Electrical Engineering, 2024, 41(10).